

Effect of temperature on the characteristics of ZnO nanoparticles produced by laser ablation in water

ELMIRA SOLATI and DAVOUD DORRANIAN*

Laser Laboratory, Plasma Physics Research Center, Science and Research Branch, Islamic Azad University, Tehran, Iran

MS received 9 January 2016; accepted 19 April 2016

Abstract. Effect of the water temperature on the characteristics of zinc oxide nanoparticles (NPs) produced by laser ablation process is investigated experimentally. The fundamental wavelength of a Q-switched Nd:YAG laser was employed to irradiate a high-purity zinc plate in distilled water at different temperatures of 0, 20, 40 and 60°C. The produced NPs were diagnosed by UV–vis–NIR spectroscopy, X-ray diffraction method, transmission electron microscopy and scanning electron microscopy. Results show that with increase in the water temperature from 20 to 60°C, size of NPs decreases while their bandgap energy increases. Maximum ablation rate occurs at the highest temperature. Crystallinity also increases with increase in the water temperature. The abnormal behaviour of water at 0–4°C affects the NPs characteristics.

Keywords. ZnO nanoparticle; laser ablation; bandgap energy.

1. Introduction

ZnO is actually a wide bandgap semiconductor of the II–VI semiconductor group. The doping of the semiconductor is *n*-type, which is due to oxygen vacancies. This has several favourable properties like high electron mobility, good transparency, wide bandgap for semi-conductivity, high room-temperature luminescence, etc. In the form of nanoparticles (NPs), ZnO is considered as one of the most promising and novel materials because of its unique catalytic, electrical, electronic, optical and antimicrobial properties as well as its low cost and extensive applications in diverse areas [1–3]. Among several techniques laser ablation method is a clean useful method for producing NPs. This method will not produce any toxic byproduct materials. By controlling several features such as laser pulse width, laser wavelength and laser spot size as well as ablation environment characteristics, we can control the nature of the produced NPs [4–6].

There are several published works on producing ZnO NPs by laser ablation method. He *et al* [4] worked on self-assembly of ZnO NPs produced by nanosecond pulsed laser ablation (PLA) in aqueous media. They reported that small ZnO NPs were obtained by PLA of a Zn plate in aqueous media, and subsequent aging of the obtained ZnO NP suspension produced in cetyltrimethylammonium bromide solution led to the formation of spindle-like ZnO aggregates. However, the spindle-like ZnO aggregates were not observed in deionized water but fluffy round aggregates were obtained [4]. Gondal *et al* [7] worked on the synthesis of ZnO₂ NPs by laser ablation in liquid and their annealing transformation into ZnO NPs. Singh and Gopal [8] worked on the synthesis

of colloidal zinc oxide NPs by PLA in aqueous media with passing pure oxygen gas simultaneously. In their work, possible mechanism for the synthesis of ZnO and zinc oxyhydroxide NPs are discussed. Thareja and Shukla [9] worked on the characterization of ZnO NPs by laser ablation in different liquid environment. Ismail *et al* [10] worked on the preparation of colloidal ZnO NPs in water by laser ablation at different laser conditions. Fazio *et al* [11] worked on the optical and structural properties of ZnO nanostructures by laser ablation, by varying the laser pulse energy between 20 and 150 mJ, and for an ablation time of 10 min.

Following our recent works on investigation of the effects of laser wavelength, pulse energy [12] and aqueous ablation environment [13] on producing ZnO NPs, and investigation of the effects of volumetric ratio of Au and ZnO suspensions [14] and ZnO and graphene nanosheets [15] on the characteristics of ZnO NPs, we have presented the effect of ablation environment temperature on the structure and morphology of ZnO NPs produced by laser ablation method in this work. To do this, we have produced ZnO NPs in distilled water of 0, 20, 40 and 60°C temperatures.

2. Experimental

NPs were prepared by ablation of a high-purity zinc bulk in distilled water, using the fundamental wavelength of Nd:YAG laser operating at 1064 nm with pulse width of 7 ns and 10 Hz repetition rate. Zn bulk was placed at the bottom of a water container with its surface at the focal point of 80-mm convex lens. The height of water on the target was 8 mm. Laser beam diameter was 6 mm before lens and was calculated to be 50 μm on the surface of the target. The volume of the water in the ablation container was 20 ml and Zn

* Author for correspondence (doran@srbiau.ac.ir)

target was ablated with 500 laser pulses at 0.7 J cm^{-2} fluence. To study the effect of ablation environment temperature, the ablation container was placed on an automatic heater and the temperature of water was controlled by a thermometer. Samples 1–4 were produced in water at 0, 20, 40 and 60°C , respectively, which are labelled as s1 to s4 in this report.

Optical absorption spectra of samples in a 10-mm path length quartz cells were measured by UV–vis–NIR spectrophotometer from PG Instruments (T-80). Transmission electron microscopy (TEM) and scanning electron microscopy (SEM) micrographs were taken using Zeiss EM10C and KYKY-EM3200 systems, respectively. X-ray diffraction (XRD) was measured using X-PERTPRO MPD X-ray diffract-meter from the PANalitical. To measure the ablation rate in the liquid medium, the target was weighed before and after the ablation process by Sartorius Utensil model CP225D with 0.01 mg readability. After ablation inside water with 500 laser pulses, the target was dried and weighed again. Hence, the mass loss of the target attributed to the amount of generated NPs.



Figure 1. Zinc oxide nanoparticle samples produced in different water temperatures.

3. Results and discussion

Picture of samples is presented in figure 1. For NP suspension, the colour depends on the size and concentration of NPs. The colour of ZnO NP suspension in different temperatures is colourless. Variation of the temperature in our experimental condition has not changed the colour of samples. In this work, colour of suspensions is very closed and confirms the fact that the sizes of ZnO NPs produced in different temperature are very closed.

In figure 2, the ablation mass of samples vs. water temperature is plotted. To achieve this data, dried target was weighted before and after the ablation process. Difference of these two weights is the reduced mass of target. Results show that the minimum ablated mass occurs when the temperature of water as the ablation environment was 20°C for sample 2. Increase in the water temperature, more than 20°C , leads to increase in the rate of ablation in our experimental condition.

XRD spectra of NPs as well as the XRD pattern of the Zn target are presented in figure 3. In order to do this measurement, samples were dried on the copper foil at room temperature. The XRD spectrum clearly shows the crystalline structure of the NPs and various peaks of zinc oxide. We have the multi-structure of NPs indicating that their peaks intensity is changed for different samples. From sample 1 to sample 2 the intensity of XRD peaks is decreased, while from sample 2 to sample 4 the intensity of peaks is increased. The intensity of the peaks increases with increase in temperature, indicating increased crystallinity. The XRD peaks of NPs occurred at very similar angles, and most of them were different with Zn target peaks. It can be concluded that Zn and O atoms are composed during the ablation process. Ablation of atoms has taken place and nucleation occurred during the plasma plume expansion phase on the surface of target. The dynamics of a cavitation bubbles was also controlled by changing the temperature of water as a liquid medium.

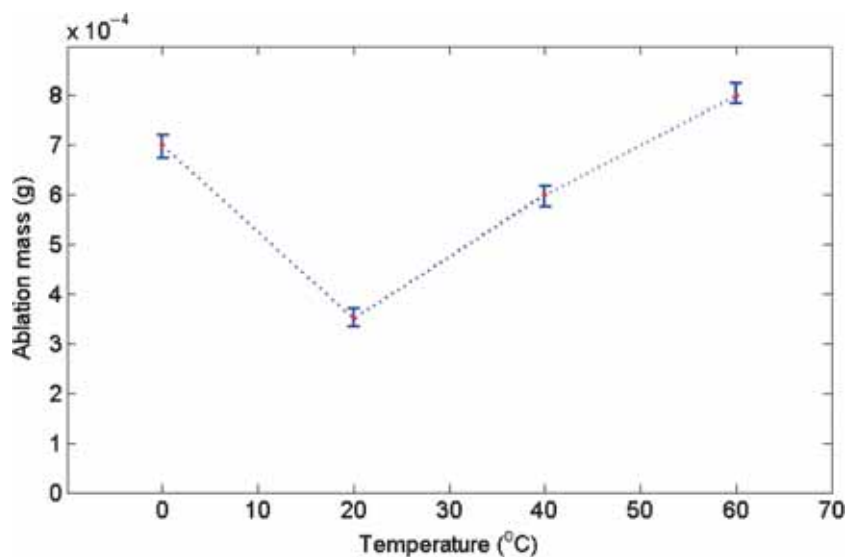


Figure 2. Variation of the ablation mass in different temperatures.

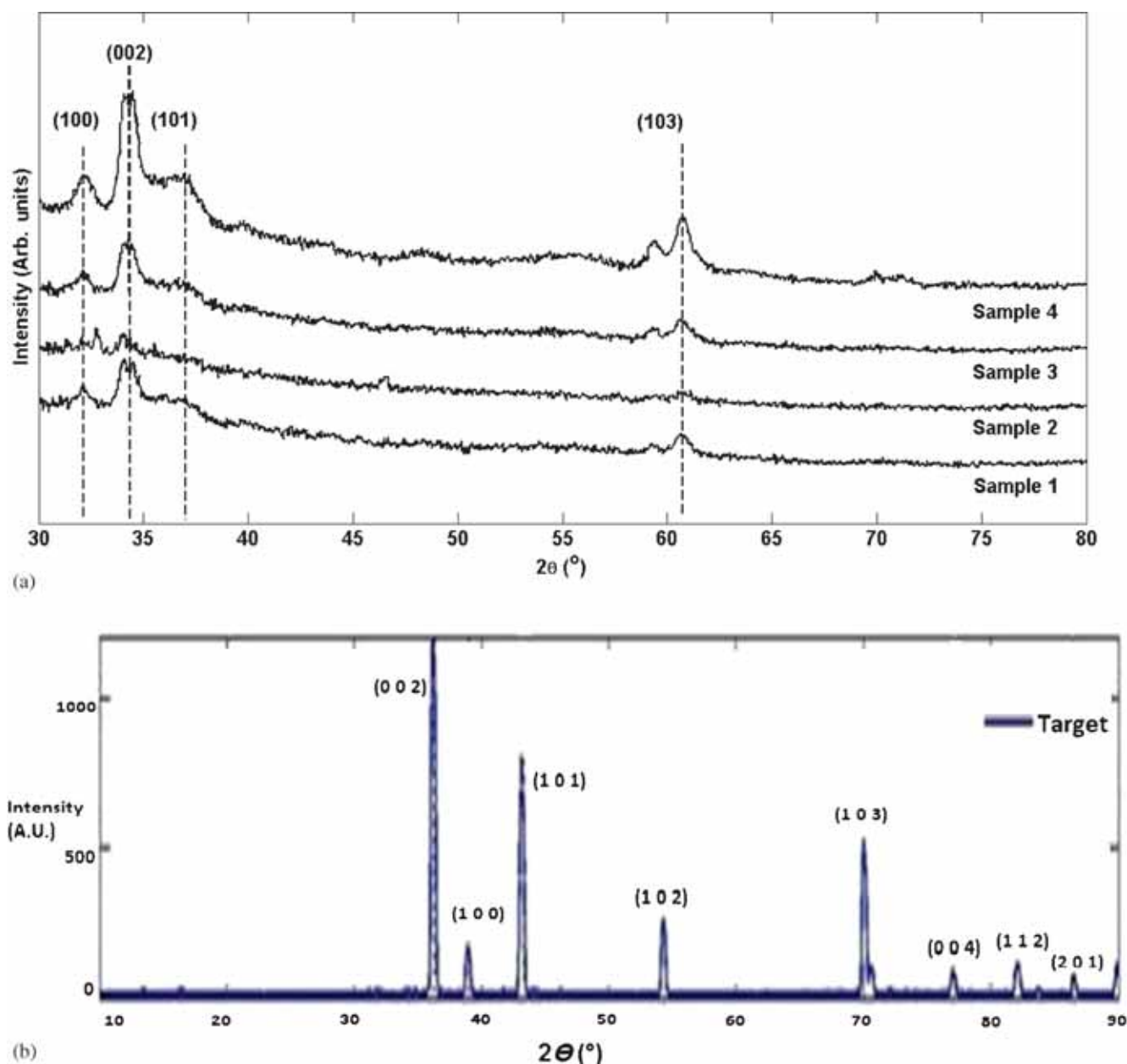


Figure 3. X-ray diffraction pattern of (a) zinc oxide nanoparticle and (b) zinc target.

The XRD pattern of the ZnO NPs in water at different temperature reveals that they possess the hexagonal wurtzite structure. Results are in good agreement with other reports, which are mostly on the production of ZnO NPs by laser ablation in water [2]. The average grain size D of the NP of ZnO generated by laser ablation was estimated by using the standard Equation (1), known as Scherrer formula [16]:

$$D = \frac{k\lambda}{\beta \cos \theta}, \quad (1)$$

where k is a constant ($0.89 < k < 1$), λ wavelength of the X-ray, β the FWHM (full-width at half-maximum) of the diffraction peak and θ the diffraction angle. The mean grain size of NPs are calculated using FWHM of peak at $2\theta = 34.5^{\circ}$, listed in table 1. The grain size extracted using Scherrer formula is the average grain size of (002) planes of ZnO

Table 1. Introduction of samples.

Sample	s1	s2	s3	s4
Water temperature ($^{\circ}$ C)	0	20	40	60
Grain size (nm) extracted from Scherrer formula using XRD peak	9.24	9.23	10.26	10.26
Absorption peak wavelength (nm)	291	293	292	291
Bandgap energy (eV)	3.93	3.82	3.91	3.96

nanostructures. Result shows that the mean grain size of ZnO NPs produced in different temperature are very close. The differences between the grain sizes of NPs prepared in various temperatures are very small, which is justified to measure with such high precision. On the other hand, at higher temperatures of water, migration of grain boundaries occurs,

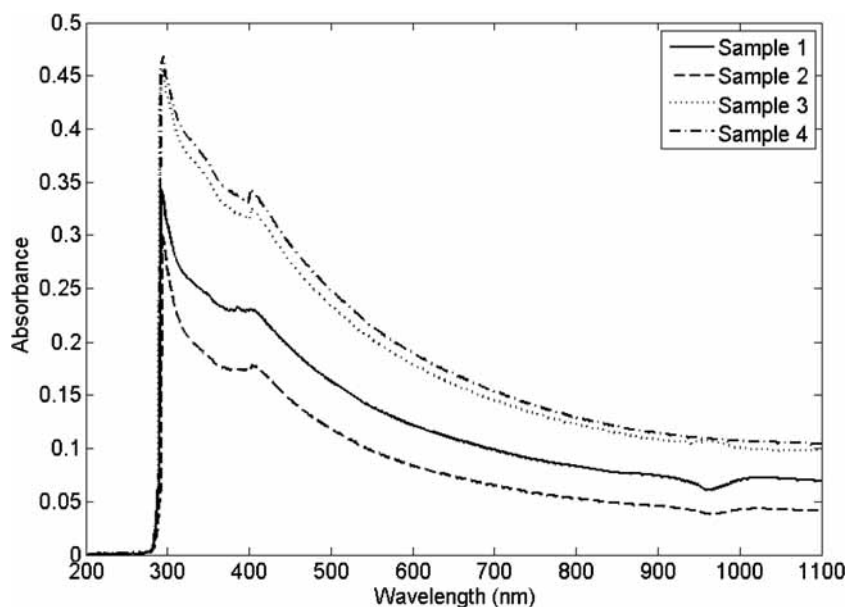


Figure 4. UV-vis-NIR absorption spectrum of zinc oxide nanoparticles produced in different temperatures.

causing the coalescence of small grains and formation of large grains.

Absorption spectra of NP solutions in the range of 200–1100 nm are presented in figure 4. The resonance absorption peaks at 291–293 nm due to ZnO NPs exciton resonance absorption can be observed. It can be seen that the intensity of absorption peaks and their FWHMs are different for samples. The intensity of peaks is decreased from s1 to s2, while it is increased with increase in the temperature from s2 to s4. The intensity of peaks is directly proportional with the number of particles in suspensions, as is presented in figure 2. The smallest intensity of s2 confirms that the amount of NPs in this sample is smaller than others. The most dramatic property of semiconductor NPs is the size evolution of the optical absorption spectra. Hence UV-visible absorption spectroscopy is an efficient technique to monitor the optical properties of quantum-sized particles [17]. If the size of NPs increases, their resonance absorption spectrum peak will be shifted towards larger wavelength and vice-versa. For exciton resonance phenomenon to happen, the particle must be much smaller than the wavelength of incident light. A red shift in the absorption spectrum is due to increase in the average NP size in samples, that the absorption measurements provide a qualitative indication of the crystal size distribution. The sharp excitonic peak at lower water temperature shows the narrow size distribution of the NPs in the samples. At higher temperature, sharp excitonic features are not present in the absorption spectra. This is due to the fact that a number of exciton peaks appear at different energies, corresponding to different size nanocrystals which overlap with each other. Therefore, a broadened size distribution of the nanocrystals can be expected. This assumption is confirmed by the number size distributions recorded by using other diagnostics. The wavelengths corresponding to excitonic

absorption peaks are presented in table 1. Here also from s1 to s2 we have a red shift, while from s2 to s4 a blue shift is observed. This observation confirms that with increase in the temperature from s1 to s2 the size of NPs increased, while with increase in the temperature from s2 to s4 the size of NPs decreased. According to the width of the absorption peak, variety of particle size distribution increases with increase in the water temperature.

The absorption coefficient spectrum of samples vs. photon energy is presented in figure 5. This spectrum is deduced from transmission spectrum of samples in Beer-Lambert law equation;

$$I = I_0 e^{-\alpha d}, \quad (2)$$

where I is the intensity of the light passing through the sample cell, I_0 the intensity of the light passing through the reference cell, α the absorption coefficient and d the distance between sides of cell. For measuring the transmission spectrum, samples were in a 1 cm² quartz cells. According to this figure, the peak can be observed at about 4.25 eV. Nature of the small peak at about 3 eV is not clear for us.

The influence of nanocrystal size on the electronic structure of semiconducting material is represented by the bandgap increase with decrease in the particle size, which is attributed to the so-called quantum confinement effect. Using absorption spectrum in Tauc equation, the bandgap energy of samples is calculated [18,19]. Tauc equation is as follows:

$$\alpha h\nu = B(h\nu - E_g)^m, \quad (3)$$

where α is the absorption coefficient, $h\nu$ the photon energy, E_g the bandgap energy and B a factor that depends on the transition probability and can be assumed to be constant within the optical frequency range. The index m is related to the distribution of the density of states. The index m has

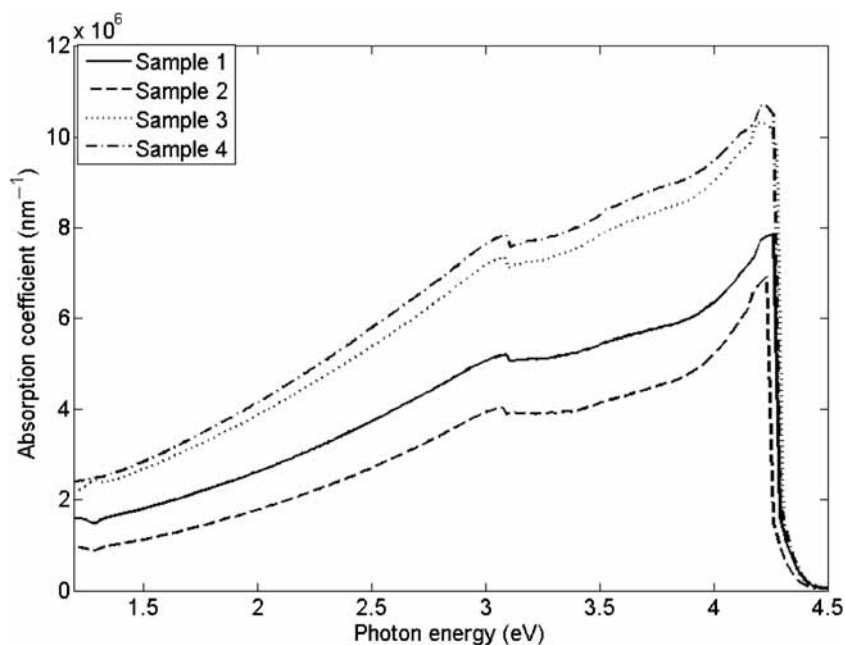


Figure 5. Absorption coefficient of nanoparticles.

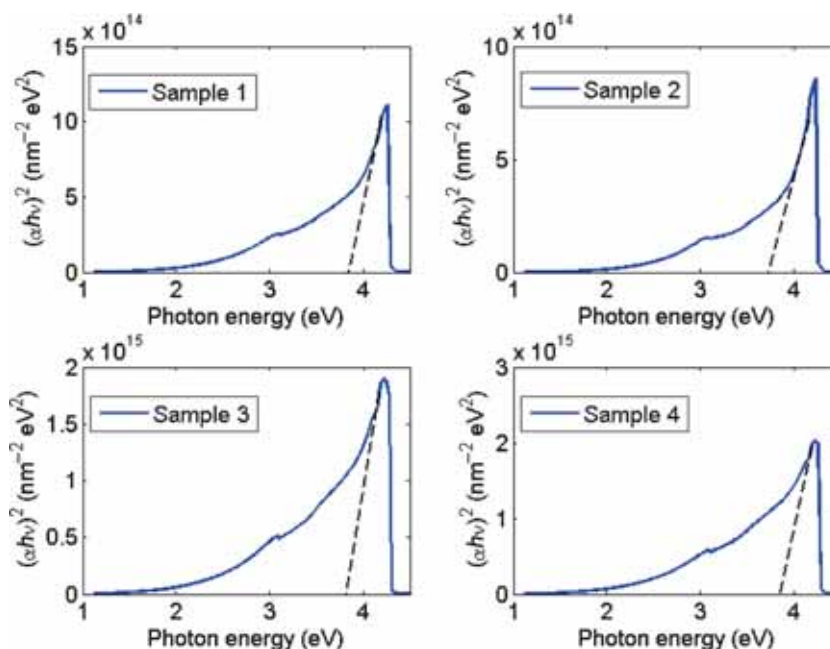


Figure 6. Plot of $(\alpha h\nu)^2$ vs. photon energy to extract the bandgap energy of samples, where α is the absorption coefficient and $h\nu$ the photon energy.

discrete values like $1/2$, $3/2$, 2 , more depending on whether the transition is direct or indirect and allowed or forbidden, respectively. In the direct and allowed cases the index $m = 1/2$, whereas for the direct but forbidden cases it is $3/2$. However for the indirect and allowed cases $m = 2$ while for the forbidden cases it is 3 or more [20]. The value of m for our samples is estimated from the slope of the $\log(\alpha)$ vs. $\log(h\nu)$ plots by taking a linear fit and is found to be $1/2$. To calculate E_g , the usual method is plotting $(\alpha h\nu)^{1/m}$ against $h\nu$, which is presented in figure 6. The values of the bandgap energies of samples are found to be 3.82 – 3.96 eV, which is presented

in table 1. Similar result has been reported by Solati *et al* [12]. From s1 to s2 the bandgap energy is decreased, while from s2 to s4 the energy of bandgap is increased. The bandgap energy of NPs strongly depends on their size and morphology. In any case, the bandgap energy of NPs is larger than the bulk material. In fact, higher temperature leads to larger kinetic energy that increases collision among initially formed large NPs in the condensation process and NPs are placed in the path of the laser beam, and fragmentation phenomena may also take place which further reduces the size of NPs.

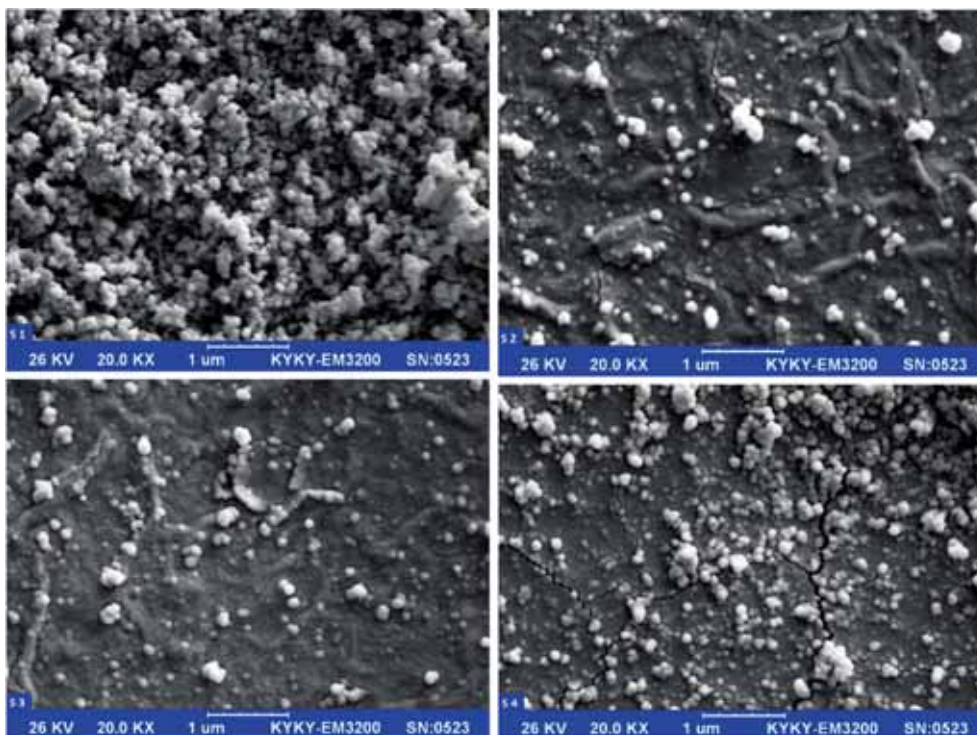


Figure 7. Scanning electron microscopy images of nanoparticles dried on silicon substrate.

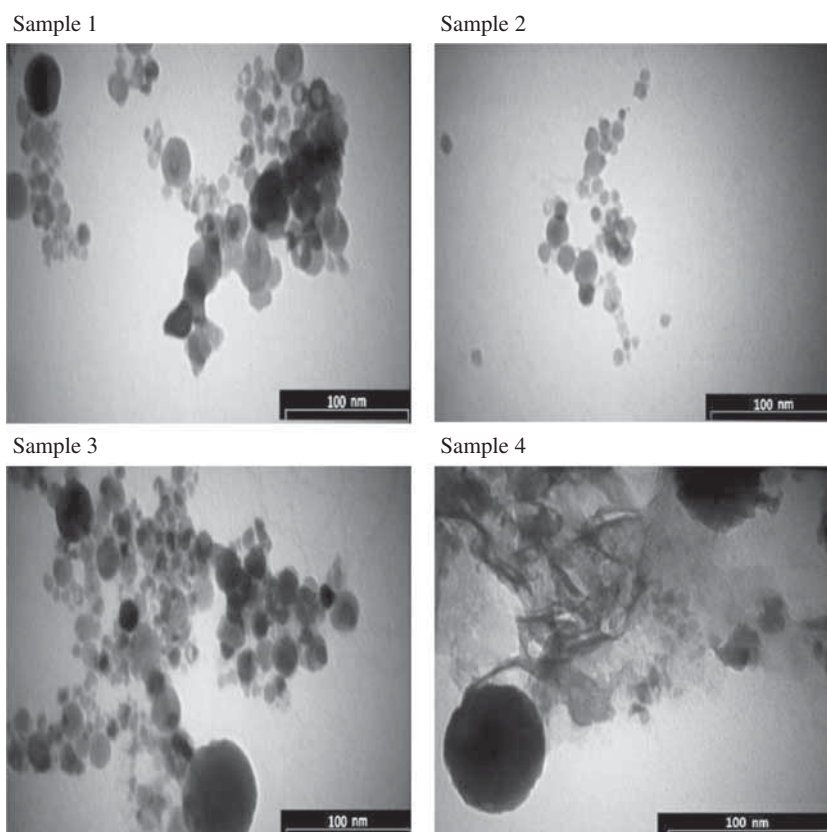


Figure 8. Transmission electron microscopy images of nanoparticles.

SEM images of ZnO NPs prepared by laser ablation method in water at different temperatures are shown in figure 7. Images are taken using 26 keV electrons and 20 kX magnification. For SEM imaging, few drops of suspensions were dried on silicon substrate at room temperature. Morphology of ZnO NPs in this experimental condition does not depend on the water temperature. The produced NPs in all samples are spherical. These images confirm that the minimum production rate occurs when the temperature of water was 20°C. Aggregation of particles decreases with increase in the water temperature. In comparison with results reported in Ref. [12], the particles prepared by laser pulse of 1064 nm wavelength are sheet-like and spherical nanostructures and size and amount of sheet-like nanostructures decreased by increase in the laser pulse energy. According to the Ref. [21], the ZnO NPs prepared by ablation at 40°C were almost spherical and adhered to each other, but particles prepared at 60 and 80°C were observed in the small polyhedron and rod-like nanostructures.

TEM images of the NPs in the scale of 100 nm are displayed in figure 8. Figure 9 also shows the size distribution of ZnO NPs. Size distribution profiles are measured using MEASUREMENT software. The products are composed of the particles with nearly spherical shape, like other reports [21,22]. The particle sizes and size distribution are related to the environment temperature. As can be seen, the size of NPs increases from s1 to s2, and then decreases with increase in the water temperature. Average diameters of ZnO NPs varied from about 9.84, 10.69, 9.80 and 6.55 nm for samples 1–4, respectively. One can clearly see that the size of NPs shifts towards smaller particles size with increase in the temperature of water, because high temperature of water can supply more kinetic energy to the NPs during the laser irradiation. In this process, ZnO NPs are placed in the path of the laser beam, and fragmentation phenomena may also take place due to the interaction between pulsed laser light and colloids, thus reducing the final particle size of ZnO NPs. Result

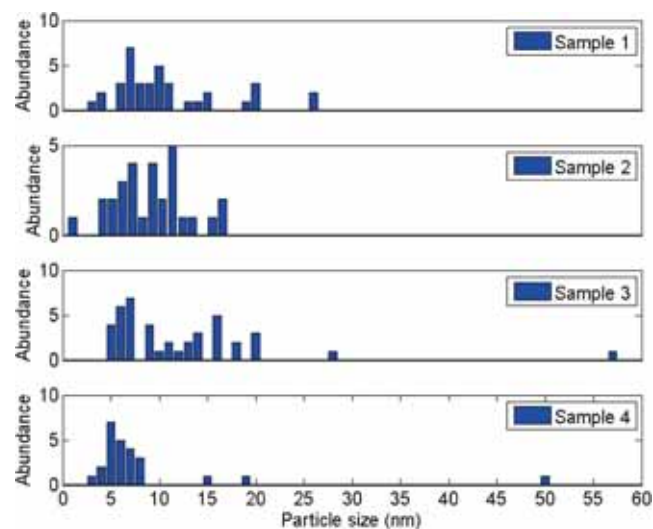


Figure 9. Size distribution of zinc oxide nanoparticles extracted from transmission electron microscopy.

shows that with increase in the water temperature the size distributions of ZnO NPs is rather wide. TEM micrographs show that some NPs consist of a black core with grey shells. If we consider the black cores as the non-oxide Zn atoms, the grey shells indicate ZnO; small NPs are ZnO.

4. Conclusion

ZnO NPs were prepared by pulse laser ablation method in water as a liquid environment, because of its potential to control the features of NPs. In this work, the effect of ablation environment temperature on the structure, morphology and optical properties of ZnO NPs have been investigated. XRD data reveal that these NPs possessed the hexagonal wurtzite structure. Blue shift in peak of absorption spectrum of ZnO NPs and TEM images showed that the particle size of ZnO NPs is decreased with increase in the temperature of water. SEM image indicates that the morphology of ZnO NPs was spherical and does not affect with the variation of temperature in this range. Bandgap energy of samples was changed in range with their size; i.e., the bandgap energy was decreased from s1 to s2 and increased from s2 to s4. Actually, higher temperature leads to larger kinetic energy that increases collision among initially formed large NPs in the condensation process and NPs are placed in the path of the laser beam, and fragmentation phenomena may also take place which further reduces the size of NPs.

References

- [1] Ou Q, Shinji K, Ogino A and Nagatsu M 2008 *J. Phys. D: Appl. Phys.* **41** 205104
- [2] Dorrnian D, Solati E and Dejam L 2012 *Appl. Phys. A* **109** 307
- [3] Raoufi D 2013 *J. Lumin.* **134** 213
- [4] He Ch, Sasaki T, Shimizu Y and Koshizaki N 2008 *Appl. Surf. Sci.* **254** 2196
- [5] Solati E, Mashayekh M and Dorrnian D 2013 *Appl. Phys. A* **112** 689
- [6] Solati E and Dorrnian D 2015 *J. Cluster Sci.* **26** 727
- [7] Gondal M A, Drmsh Q A, Yamani Z H and Saleh T A 2009 *Appl. Surf. Sci.* **256** 298
- [8] Singh S C and Gopal R 2008 *Physica E: Low Dimens. Syst. Nanostruct.* **40** 724
- [9] Thareja R K and Shukla S 2007 *Appl. Surf. Sci.* **253** 8889
- [10] Ismail R A, Ali A K, Ismail M M and Hassoon K I 2011 *Appl. Nanosci.* **1** 45
- [11] Fazio E, Mezzasalma A M, Mondio G, Neri F and Saija R 2013 *Appl. Surf. Sci.* **272** 30
- [12] Solati E, Dejam L and Dorrnian D 2014 *Optics Laser Technol.* **58** 26
- [13] Moradi M, Solati E, Darvishi S and Dorrnian D 2016 *J. Cluster Sci.* **27** 127
- [14] Mehrani A, Dorrnian D and Solati E 2015 *J. Cluster Sci.* **26** 1743

- [15] Solati E and Dorrnian D 2016 *Appl. Phys. B* **122** 76
- [16] Suryanarayana C and Norton M G 1998 *X-ray diffraction a practical approach* (New York: Plenum Press)
- [17] Srinivasa Rao B, Rajesh Kumar B, Venkata Chalapathi G, Rajagopal Reddy V and Subba Rao T 2011 *J. Nano Electronic Phys.* **3** 620
- [18] Yakuphanoglu F, Barim G and Erol I 2007 *Physica B: Condens. Matter* **391** 136
- [19] Saravanan S, Anantharaman M R, Venkatachalam S and Avasthi D K 2007 *Vacuum* **82** 56
- [20] Yakuphanoglu F and Arslan M 2007 *Physica B: Condens. Matter* **393** 304
- [21] Ishikawa Y, Shimizu Y, Sasaki T and Koshizaki N 2006 *J. Colloid Interface Sci.* **300** 612
- [22] Zeng H, Cai W, Li Y, Hu J and Liu P 2005 *J. Phys. Chem. B* **109** 18260